Transworld Research Network
37/661 (2), Fort P.O.
Trivandrum-695 023
Kerala, India

Experimental and Theoretical Studies in Modern Mechanochemistry, 2010: 000-000
ISBN: 978-81-7895-454-7 Editors: Francesco Delogu and Gabriele Mulas

3. Apparent and hidden mechanochemistry

Valery I. Levitas
Department of Mechanical Engineering, Department of Aerospace Engineering, Department of Material Science and Engineering 2008 Black Engineering Building Iowa State University Ames, Iowa 50011-2161, USA

Abstract. Two phenomena will be considered. Phase transformations (PTs) and chemical reactions (CRs) under compression and shear of materials in rotational diamond anvil cell (RDAC) represent examples of apparent effects of plastic shear. We recently predicted the new phenomenon that crystal-crystal and crystal-amorphous PTs can occur through virtual melting (*VM*) significantly below (> 1000*K*!) the melting temperature. This hidden mechanochemical phenomenon is caused by the energy of the internal elastic stresses, induced by solid-solid PT. It increases the driving force for melting and reduces the melting temperature. Melting releases the stresses, and the unstable melt solidifies into the crystalline or amorphous phase (above or below the glass transition temperature, respectively). Some indications were found about the existence of the *virtual amorphization* (*V A*), and that *VM* and/or *V A* may serve as mechanisms of various structural changes: plastic flow under high-strain-rate and shock loading of HMX crystal, metals, and metallic nanowires; fracturing; nanofriction; sublimation; and grain growth and sliding. One more example of hidden mechanochemistry is related to the melt-dispersion mechanism of the reaction of Al nanoparticles.

Correspondence/Reprint request: Dr. Valery I. Levitas, Department of Mechanical Engineering, Department of Aerospace Engineering, Department of Material Science and Engineering 2008 Black Engineering Building Iowa State University Ames, Iowa 50011-2161, USA. E-mail: vlevitas@iastate.edu

1. Introduction

Mechanochemistry studies the effect of nonhydrostatic stresses and plastic strain on structural changes (SCs) which include PTs and CRs. In this paper, we will review our recent work on high pressure mechanochemistry (where the plastic shear is an apparent reason for intensifying the SCs) and on the *V M* as a mechanism of PTs and stress relaxation in the solid, which is caused by internal nonhydrostatic stresses. Since internal stresses appear unintentionally due to a change in volume during the crystal-crystal PT (rather than due to purposeful action of experimentalists), we will call their effect a ”hidden” mechanochemistry. Due to a lack of space, we will cite, in many cases, our comprehensive or review papers where detailed references on original works are given.

2. High pressure mechanochemistry

Phenomena. After compression of the materials in Bridgman or diamond anvils, a very high pressure is produced in the specimen which leads to a number of SCs. It is known, from numerous experiments obtained by Bridgman, Vereschagin, Enikolopyan, Blank, Zharov and coauthors, that in rotating Bridgman or diamond anvils the addition of plastic shear, due to the rotation of an anvil, leads to findings that have both fundamental and applied importance; they are reviewed in detail in [1, 2].

1. Plastic shear leads to a significant (in some cases by a factor of 3-5) reduction of transformation [3, 4] and reaction [5] pressure. 2. It also leads to the formation of new phases which were not produced without shear. 3. The volume fraction of the product phase or the reaction product is an increasing function of the plastic shear strain. Therefore, strain-controlled (rather than time-controlled) kinetics is considered. 4. Plastic shear reduces pressure hysteresis, i.e. the difference between the start pressure of direct and reverse transformation, in some cases to zero. From this, it was claimed that the obtained transformation pressure can be interpreted as an equilibrium pressure. 5. In some cases, shear deformation substitutes a reversible transformation with an irreversible transformation. Consequently, it allows production of phases which are metastable at normal pressure and can be used in engineering applications.

Until recently, there were no publications that explain and characterize any one of the above mechanochemical phenomena. Even the basic difference between the plastic *strain-induced SCs under high pressure and pressure-induced SCs* has not been recognized. Pressure- and stressinduced SCs occur predominantly at pre-existing defects at stress levels below the

yield strength while strain-induced SC occurs by nucleation at new defects generated during plastic flow. Strain-induced SCs require a completely different experimental characterization as well as thermodynamic and kinetic description.

The first multiscale theory of strain-induced SCs. A general thermomechanical description of SCs in elastoplastic materials which we developed during the last several years is presented in [1, 6, 7]. In an attempt to explain the phenomena enumerated above, we developed a first multiscale theory of strain-induced SCs [1, 2] that has been verified by various experimental findings. At the nanoscale, the primary reason for the above phenomena is related to the generation of new defects during plastic flow. These defects produce regions of strong stress concentration and serve as new nucleation sites. Accordingly, a model of nucleation at the tip of dislocation pile-up was developed. The corresponding geometric parameters and orientation of nucleus were determined. It was demonstrated that shear stress can lead to substitution of thermally activated nucleation with barrierless nucleation and significantly reduces the SC pressure for direct SC, as well as increases it for reverse SC. Barrierless nucleation explains the strain-controlled rather than time-controlled kinetics. As straining stops, no new defects or nuclei appear, and the growth of the existing nuclei is thermodynamically impossible. This also explains the nanoscale size of the formed grains which are produced by strain-induced nucleation. The model confirms that the introduction of plastic shear, under high pressure, reduces the SC stresses by a factor of 2-10 or possibly more. Dislocation pile-ups generate both compressive and tensile stresses of the same magnitude. Consequently, they simultaneously promote both direct and reverse SC in different regions. All of the above findings were conceptually incorporated into the microscale model.

At the microscale, a new strain-controlled kinetic equation is derived based on our thermo-dynamic SC criterion. The equation considers the possibility of direct and reverse PT and the difference in the plastic strain in each phase due to the different yield strength of the phases. A stationary and nonstationary solutions of this equation are found and analyzed. The stationary solution explains the zero pressure hysteresis observed experimentally as well as the appearance of new phases; especially the strong phases, which were not obtained without the plastic shear. However, the zero hysteresis can be obtained at any pressure in a specific range and has nothing to do with phase equilibrium pressure. The phase equilibrium pressure does not appear in any of the equations and cannot be obtained from experiments on strain-induced SC. Also an explanation was obtained why a nonreacting matrix with a yield strength higher (lower) than that for reagents significantly

accelerates (slows down) the reactions. Recently [8], this theory was generalized for an arbitrary number of phases and applied to strain-induced PTs between three phases in Ge and Si.

At the macroscale, mechanics of plastic flow and SC in a rotating diamond anvil was modeled analytically. A strain-controlled kinetic equation derived at the microscale was used. The sliding of the rotating anvil with respect to material was determined. The promotion of the SC due to the rotation of the anvil was found to be related to the reduction of the radial component of shear friction stress. This led to additional axial displacement, which balanced the volume decrease due to SC, and increased the plastic strain and pressure. If the new phase has a larger yield strength, pressure grows in the transforming regions; this explains and quantifies the pressure self-multiplication effect (i.e. growth of the pressure at the center of a sample under fixed applied force) observed experimentally [1, 2, 3, 4]. Additionally, the rotation of an anvil can led to formation of new hard phases, which cannot be obtained without it. Recently, plastic flow and the evolution of distribution of the components of stress tensor in a sample under compression and shear in RDAC were studied using the finite-element method [9]. This work reveals very strong concentration of plastic strain near the contact surface between the sample and diamond and suggests that new strain-induced phases can be more easily detected in the contact layer. Our multiscale theory predicts the unique potential of the RDAC to produce high-strength metastable nanostructured phases.

Alternative macroscopic methods to promote SCs. Based on our results, we were able to formulate and implement some new methods of controlling of PT and CR under plastic deformation; some of these methods *did not require the rotation of the anvil* as the means to produce plastic shear [1, 2]. Some of them have experimental confirmations. Here, we will discuss one of the most important result. For rhombohedral rBN or hexagonal hBN single crystals that deform by slip on the basal plane only, the theoretical compressive yield strength varies from infinity, in compression along the C-axis, to a minimum value when the basal plane and slip direction are at 45^o to the compression direction. If a single crystal is compressed in a diamond anvil, along an axis with a small deviation from the C-direction, the crystal deforms in a manner that cause the C-axis to significantly deviate from the loading axis. This large deviation will lead to a reduction of the yield strength in the direction of compression (rotational softening and instability), to a reduction of disk thickness and consequently plastic straining under the constant loading force. Indeed, the following experimental results were obtained [10, 11]. A highly textured rBN was compressed along the [0001].

An abrupt irreversible martensitic PT from rBN to superhard cubic cBN PT was recorded at the sample center at a pressure of 5.6 GPa just before the PT. The thickness of the disc decreased by a factor of 10. In comparison, under hydrostatic loading, the irreversible PT rBN→cBN occurs at 55 GPa. Thus a reduction of PT pressure, *by one order of magnitude has been achieved*. We concluded in [11] that a new phenomenon, namely *PT induced by rotational plastic instability* takes place. We expect that additional rotation of an anvil will further reduce the PT pressure.

Recent experimental research with RDAC [12, 13, 14]. The first in situ synchrotron X-ray diffraction tests with RDAC were performed at the National Synchrotron Light Source at Brookhaven National Laboratory. The strain-induced disordering and PT from hBN to superhard wurtzitic wBN were studied up to 25 GPa (figure 1). In contrast to all previous studies on strain-induced PTs, in which a significant gradient in pressure forms before and during PT, we predicted theoretically and verified experimentally the conditions for an almost homogeneous pressure distribution through the PT process. This is extremely important for a quantitative characterization of the PT process. Also, the homogeneous pressure self-multiplication effect was

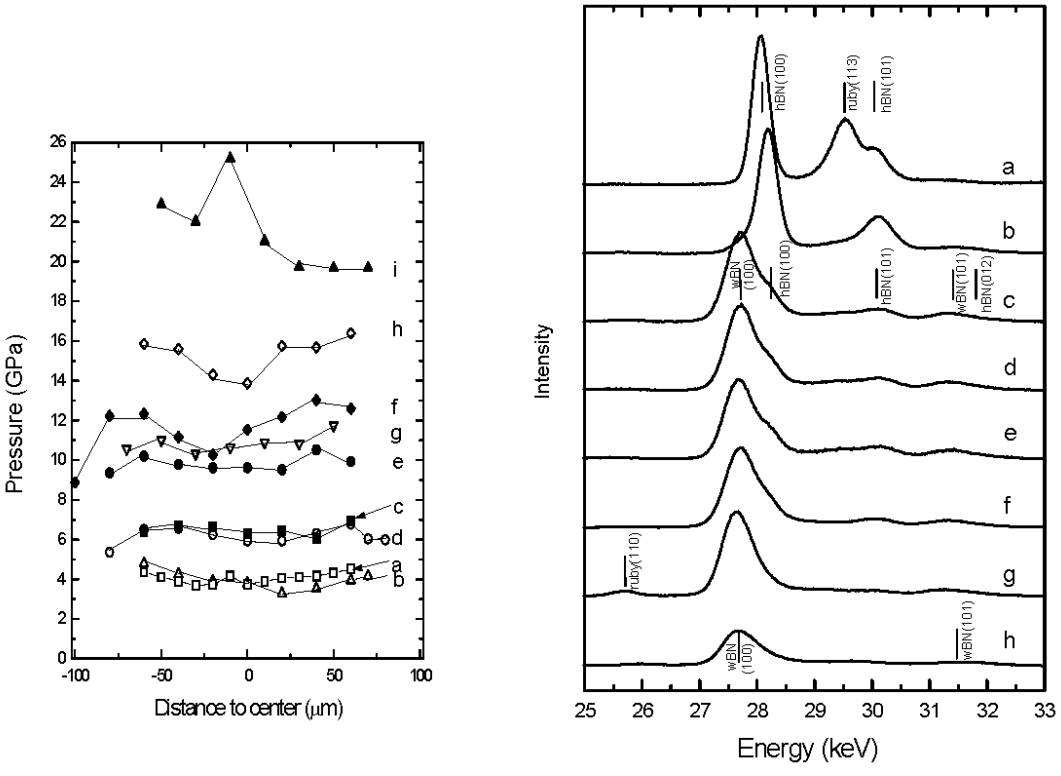

Figure 1. Pressure distribution and x-ray diffraction patterns for strain-induced phase transformation from hexagonal to wurtzitic BN in RDAC [13].

revealed, i.e. homogeneous pressure growth during the hBN→wBN PT (despite the volumetric compression of 0.53).

However, a contradictory result was obtained: although we anticipated PT at a lower pressure than hydrostatic experiments, the hBN→wBN PT under pressure and shear started at approximately the same pressure p~10 GPa as that under hydrostatic conditions. We found that under hydrostatic pressure, changes in concentration of turbostratic stacking faults, i.e. degree of disorder, were negligible. However, under a complex compression and shear loading program, a large degree of strain-induced disorder was revealed and quantitatively characterized. The results indicated that the strain-induced disorder formed during early stages of compression and shear, in turn, suppressed the PT; this resolved the contradiction. Furthermore, during the strain-induced PT, the existence of transformation-induced plasticity (TRIP) phenomenon was proved. TRIP occurs because large change in volume during PT produces huge internal stresses which in combination with external stresses cause additional plastic flow. The degree of disorder is suggested as a *physical measure of plastic straining which also allows us to quantitatively separate the conventional plasticity and TRIP*. In our experiments, *TRIP exceeded the conventional plasticity by a factor of 20*. For the same degree of disorder, *plastic shear indeed reduced the PT pressure by a factor of* 3-4, as well as caused a complete irreversible PT [13]. Strain-induced PT in iron was studied as well [14].

3. Virtual melting as a possible new mechanism for various structural changes in solids

Inelastic deformation of materials under the action of external load includes dislocation generation and motion, twinning, and fracture. The same mechanisms of inelastic deformation and internal stress relaxation can operate when stresses arise due to solid-solid PTs. Internal stresses are caused by the transformation strain tensor ε^t, which transforms the unit cell of the parent crystalline phase 1 into the unit cell of the product phase 2. We will consider the situations when classical plasticity and fracture are suppressed.

We recently predicted [15, 16, 17] the new phenomenon that crystal-crystal ($c-c$) and crystal-amorphous ($c-a$) phase transformations can occur through virtual melting ($V\,M$) significantly below ($> 1000K$!) the melting temperature. The energy of the internal elastic stresses, induced by solid-solid PT, increases the driving force for melting and reduces the melting temperature. Melting releases the stresses, and the unstable melt solidifies into the crystalline or amorphous phase (above or below the glass transition temperature, respectively). Melt in each transforming material point exists for

an extremely short time sufficient for stress relaxation, and it is a transitional activated state rather than real (thermodynamically stable) melt. We called this state the *virtual melt*. Some indications were found about the existence of the *virtual amorphization* (*V A*), and that *V M* and/or *V A* may serve as mechanisms of various structural changes: plastic flow under high-strain-rate and shock loading of HMX crystal, metals, and metallic nanowires; fracturing; nanofriction; sublimation; and grain growth and sliding.

3.1. Internal stress-induced virtual melting in energetic crystal HMX [15, 17, 18]

Let the $c - c$ PT occur in a thin layer V_n by propagation of the coherent interface. Transformation strain and coherent interface generate elastic energy $g_e > 0$, which reduces the driving force for PT. Also, a moving interface between two solids experiences resistance K due to the interaction with the stress field of crystal lattice defects. After melting in the V_n, the interface is incoherent, and elastic energy is negligible. For the melting in the V_n, $K = 0$, because liquid, as the hydrostatic medium, does not interact with the stress field of crystal defects; consequently, the *athermal resistance to interface propagation is absent*. The elastic energy before melting g^e disappears after melting, thus *increasing the driving force for melting*. We also found that the change in surface energy is negative during the melting, i.e., there is *no barrier for melt nucleation due to surface energy*. Then from the condition that the driving force for melting is zero, we can determine how the melting temperature θ_m reduces due to the elastic energy. It is also found that nonhydrostatic compressive stresses promote melting in contrast to hydrostatic pressure. After melting, internal stresses relax and unstressed melt solidifies. The solidification generates tensile stresses caused by the volume reduction. During solidification, the yield stress and resistance to fracture are negligible. That is why we assume that the elastic stresses completely relax through nanocracking or void formation. Using the *V M* mechanism, interface velocity was found.

To prove the validity of the *V M*, we consider the reconstructive $\beta \leftrightarrow \delta$ PTs in the organic energetic crystal HMX [19, 20]. *Sixteen* theoretical predictions are in qualitative and quantitative agreement with experiments [15, 17, 18]. We found that, in particular: (1) Energy of internal stresses is sufficient to reduce melting temperature from 551K to 430K for the δ phase during the $\beta \rightarrow \delta$ PT and from 520K to 400K for the β phase during the $\delta \rightarrow \beta$ PT. (2) Activation energies for direct and reverse PTs are equal to corresponding melting energy. (3) Temperature dependence of the rate constant is determined by the heat of fusion; both interface kinetics and a fully physically based overall kinetic model are in very good correspondence

with our and published experiments (figure 2). (4) Conditions $K \simeq g^e \simeq 0$ for both $\beta \leftrightarrow \delta$ PTs explain zero temperature hysteresis (which is observed in contrast to all known solid-solid PT). (5) Considerable nanocracking, homogeneously distributed in the transformed material, accompanies the PT. (6) The nanocracking does not change appreciably the PT thermodynamics and kinetics for the first and the second transformation $\beta \leftrightarrow \delta$ cycles, as predicted by theory. (7) $\beta \rightarrow \alpha$ and $\alpha \rightarrow \beta$ transformations, which are thermodynamically preferable in the temperature range $382.4 < \theta < 430$ K and below 382.4 K, respectively, do not occur. (8) $\delta \rightarrow \alpha$ transformation does not occur above 400 K. Because it is difficult to imagine any other mechanism that explains all these experimental results, we concluded that $\beta \leftrightarrow \delta$ PT in the HMX crystal occurs through V M. Most of the above experimental results were considered a major puzzles in HMX polymorphism for decades. In particular, absence of temperature hysteresis for $\beta \leftrightarrow \delta$ PTs (despite the large volumetric strain, $\varepsilon_0 = 0.08$), absence of $\beta \leftrightarrow \alpha$ PTs, where they are thermodynamically preferable with respect to $\beta \leftrightarrow \delta$ PTs (despite the two times smaller $\varepsilon_0 \simeq 0.04$), and large hysteresis for $\delta \leftrightarrow \alpha$ PTs ($\varepsilon_0 \simeq 0.04$) were unexplained by known theories. Only $\beta \leftrightarrow \delta$ PTs occur via the V

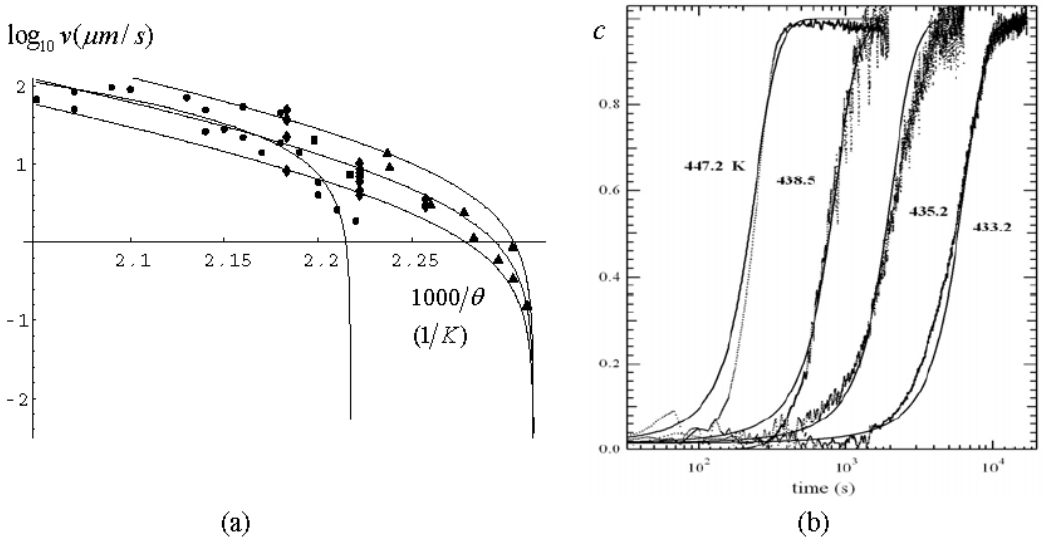

Figure 2. A comparison between theoretical prediction and experimental data for kinetics for β → δ transformation in the HMX energetic crystal under isothermal conditions [17,18]. (a) The β-δ phase interface velocity vs. temperature. Almost all symbols representing experimental data obtained at LANL and LLNL using three different methods are within a band obtained using theoretical prediction based on the virtual melting mechanism. (b) A comparison between theoretical prediction (solid curves) and experimental data for concentration of the δ phase.

M, which removes the temperature hysteresis. Volumetric strain for other PTs is not sufficient for *V M*, which explains large temperature hysteresis and suppression of some PTs due to elastic stresses and interface friction.

3.2. Crystal-amorphous and crystal-crystal transformations via virtual melting [16]

Pressure- and temperature-induced *c-a* PTs were considered (e.g., for ice, quartz, high albeite, Cd_{43} Sb_{57} and jadeite) as a low-temperature analog of melting along the continuation of melting lines in the pressure *p*-temperature θ phase diagram (figure 3). Alternatively, amorphization was related to the loss of mechanical stability of crystal lattice. However, some contradictions were found concerning metastable melting and instability hypotheses, and the mechanism of amorphization is currently not clear. In [16], we justified thermodynamically and kinetically a new mechanism of $c - a$ and $c - c$ PTs and internal stress relaxation via *VM* and *VM* induced by internal stresses. *VM* removes interface friction, reduces kinetic barrier, and increases atomic mobility.

We will consider materials with the equilibrium p-θ diagram shown in figure 3 and large volumetric transformation strain, $\varepsilon_0 > 0.1$. However, actual nonequilibrium PT lines are significantly shifted with respect to phase equilibrium

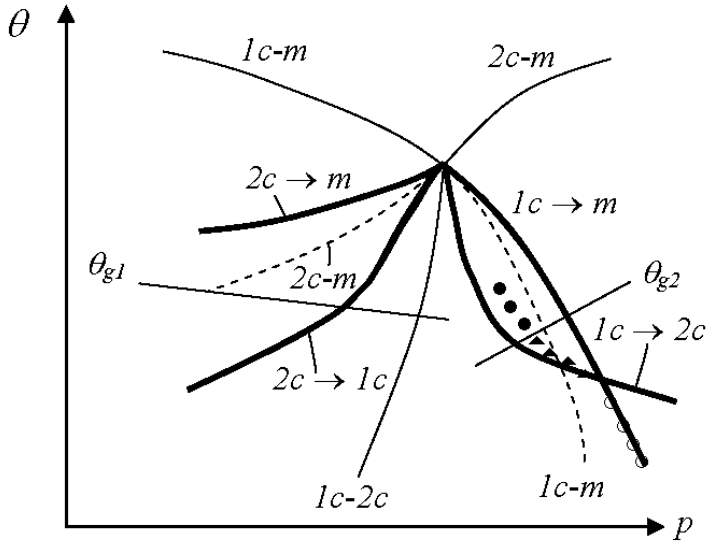

Figure 3. Equilibrium and nonequilibrium PT pressure-temperature diagrams [16]. Solid lines (*1c-m*,…) are the phase equilibrium lines. Dashed lines are metastable continuation of 1*c-m* and 2*c-m* lines. Bold lines are calculated lines for initiation of PTs. Straight lines are the glass formation temperatures θ_{g1} and θ_{g2}. ● *1c*→ internal stress-induced *VM*→2*c* PT around 2*c* nuclei; ▲ *1c*→ internal stress-induced *VM*→2*a* PT around 2*c* nuclei; ○ *1c*→ *VM*→2*a* PT.

lines due to elastic energy g^e, interface friction K, and kinetic barrier due to surface energy and diffusion [16] (figure 3). It follows from the definition of nonequilibrium PT diagram that if the loading (unloading)-heating (cooling) $p - \theta$ trajectory crosses the nonequilibrium PT line, this PT must occur. After melting $1c \rightarrow m$ in the stability region of phase 2, fast solidification will occur. Above the glass transition temperature θ_g solidification occurs to $2c$ phase; below θ_g amorphization occurs to $2a$ phase (figure 3). Usually, crystals are considered to directly vitrify into the $2a$ state, which leads to some contradictions. Consideration of VM as a separate process followed by solidification below θ_g reduces solid-state amorphization to solidification of an undercooled liquid after quenching at an infinitely fast cooling rate. This resolves some of the contradictions, in particular that the sign of heat for melting and amorphization is different, because heat of amorphization includes heat of melting $1c \rightarrow V\ M$ and solidification $V\ M \rightarrow 2a$. When the transformation line $1c \rightarrow 2c$ is crossed first, a coherent $2c$ penny-shaped nucleus appears. For suppressed plasticity, we found [16] that the elastic energy can be released by melt nucleation around the $2c$ nucleus. Since $2c$ nucleus loses its coherency, its elastic energy g_e releases, increasing the driving force for $1c - m$ PT. We also found that for in most cases the melting is barrierless. Since g_e disappears immediately as the stress in $2c$ nucleus relaxes, VM solidifies to $2c$ (above θ_g) or to $2a$ (below θ_g), producing incoherent $1c - 2c$ or $1c - 2a$ interfaces. After amorphization around $2c$ nucleus, high interface energy may transform $2c$ to $2a$ nucleus. The experimental fact that for some materials (e.g., for ice [21]) amorphization starts below the melting pressure was used as one of the main contradictions of the metastable melting hypothesis. The shift in the thermodynamic melting line resolves this seeming contradiction. Transformation lines for ice Ih [21] are located like symbols in figure 3.

The above results were applied for a new interpretation of melting, $c - c$ and $c - a$ PT mechanisms in ice Ih; we expect them to be applicable for amorphization of α−quartz and coesite, polymet, *Ge* and *Si*, jadeite, $Zn_{43}\ Sb_{57}$ and $Cd_{43}\ Sb_{57}$, BN and graphite. Note that $V\ M$ in *Si* and *Ge*, for example, occurs at more that **1000K** below the thermodynamic melting temperature! Indeed, amorphization of Si II occurs during decompression at 100K [22], while the thermodynamic melting temperature of Si exceeds 1100K in the same pressure range.

3.3. Virtual melting as a possible mechanism of various structural changes

Virtual melting and amorphization as mechanisms of plastic deformation and stress relaxation for high-strain-rate loading [23]. In our

paper [23], a new mechanism of plastic deformation and stress relaxation under very strong shock loading via the *V M* and the virtual amorphization (*V A*) several thousands K below the thermodynamic melting temperature but above the θ_g is predicted theoretically and confirmed by large-scale molecular dynamic (MD) simulations. The driving force for the melting and amorphization is due to the work and energy of nonhydrostatic stresses. After melting, nonhydrostatic stresses relax, leading to undercooled and unstable liquid under hydrostatic conditions that crystallizes. MD simulations for perfect Al and Cu crystal, shocked in [110] direction, combined with the analyzes of the stress-strain curves and thermodynamics of the process suggested the following mechanism. Disordering first leads to isotropic virtual amorphous solid. Melting of amorphous phase (that represents the second-order transformation), leads to the hydrostatically loaded *V M*. The only difference between amorphous metal and melt is the finite shear modulus. Recrystallization of the *V M* is the final process. Direct observation of the *V M* in MD simulations for plastic straining indirectly supports the plausibility the *V M* in PTs as well.

Shock loading of organic crystal HMX. A recent MD study [24] demonstrated that shock-induced deformation of α-HMX crystal occurs through homogeneous generation and motion of dislocations for shock strengths between 4.7 and 14 GPa. At higher stresses, deformation arises from formation of amorphous shear nanobands that are oriented at 45^o degrees to the loading direction and are several unit cells thick. We believe that the only currently available mechanism that may potentially explain appearance of disordered bands in a perfect elastically loaded crystal is related to stress-induced *V M*. Simplified thermodynamic modeling supports this idea.

Crystal reorientation during the nanofriction via the virtual melting. The MD simulation of the high-velocity sliding friction between two identical fcc *Al* single crystals, but along different crystallographic faces, exhibits the following phenomenon [25]. In a certain range of sliding velocities, one of the crystals melts and rapidly recrystallizes into the second orientation. The sliding interface thus moves downward, as one crystal orientation grows at the expense the other, via intermediate liquid layer.

Our simplified nonequilibrium continuum thermodynamic model suggests the following. Due to elastic anisotropy, melting temperatures, θ_{mi}, of different crystal faces under the same traction are different. When temperature at the sliding contact reaches the melting temperature of the face with $\theta_{m1} < \theta_{m2}$, it melts. However, since $\theta < \theta_{m2}$, melt is unstable with respect to crystal face 2. Because the existing face 2 supplies perfect nucleation sites

for solidification, melt solidifies into crystal structure of face 2. This is one more example of the V M phenomenon.

Virtual amorphization as a mechanism of plasticity for high-strain-rate tension of metallic nanowires. MD simulations in [26] demonstrated the following result for high-strain-rate tension of single crystal Ni and NiCu nanowires at 300 K. For 0.05% and 0.5% ps^{-1} the stress is relaxed by twin formation. For 5% ps^{-1}, the crystalline phase for both systems transforms continuously to an amorphous phase. Slowing the strain rate to 1% ps^{-1} leads to the recrystallization of the sample - i.e., it is $V\,A$. Effectively, the high strain rate has decreased the "melting" temperature from 1700 K to 300 K. The thermodynamic effect of surface energy and tension may be very important for amorphization of nanowires. Since the disordered material supports tensile stress of 3 GPa, it is amorphous solid rather than melt.

Virtual melting as a possible mechanism of fracture. In situ fracture studies on thin films of the NiTi intermetallic compound [27] revealed stress-induced amorphization of regions directly in front of moving crack tips in a temperature range 300-600 K. MD simulations in [28] suggest that fcc crystals of the metals (platinum, gold, rhodium, and silver) under uniaxial tension at temperatures above half the melting temperature disordered before they failed by void formation. We may hypothesize that disordering in both cases represents the $V\,M$.

Virtual melting as a possible mechanism for the grain boundary processes. Mott [29] suggested that the grain boundary sliding and migration occur through local melting and solidification of small groups of atoms. Kinetic analysis in [29] is oversimplified, which is why this theory was not supported by experiments. Later MD studies [30], however, demonstrated that migration of high-angle grain boundary involves "melting" of small groups of atoms and collective reshuffling followed by crystallization onto the other crystal. Other MD simulations [31] demonstrated the possibility of a reversible, smooth transition in high-energy grain boundary from solid crystalline structure to liquid confined structure above θ_g and below θ_m. The results were obtained for silicon and fcc metals. Grain boundary diffusion involves thermally activated formation of liquid-like clusters from the disordered phase and liquid-like atom migration within clusters. As a consequence, grain-boundary diffusivity and mobility occur with activation energies related to the liquid state. When temperature falls below θ_g, the melt solidifies to an amorphous state, the energy of which is 15% lower than the energy of the initial crystalline structure of the grain boundary. For recrystallization, a similar mechanism of melt nucleation at the intersection of several grain boundaries followed by crystallization can be considered.

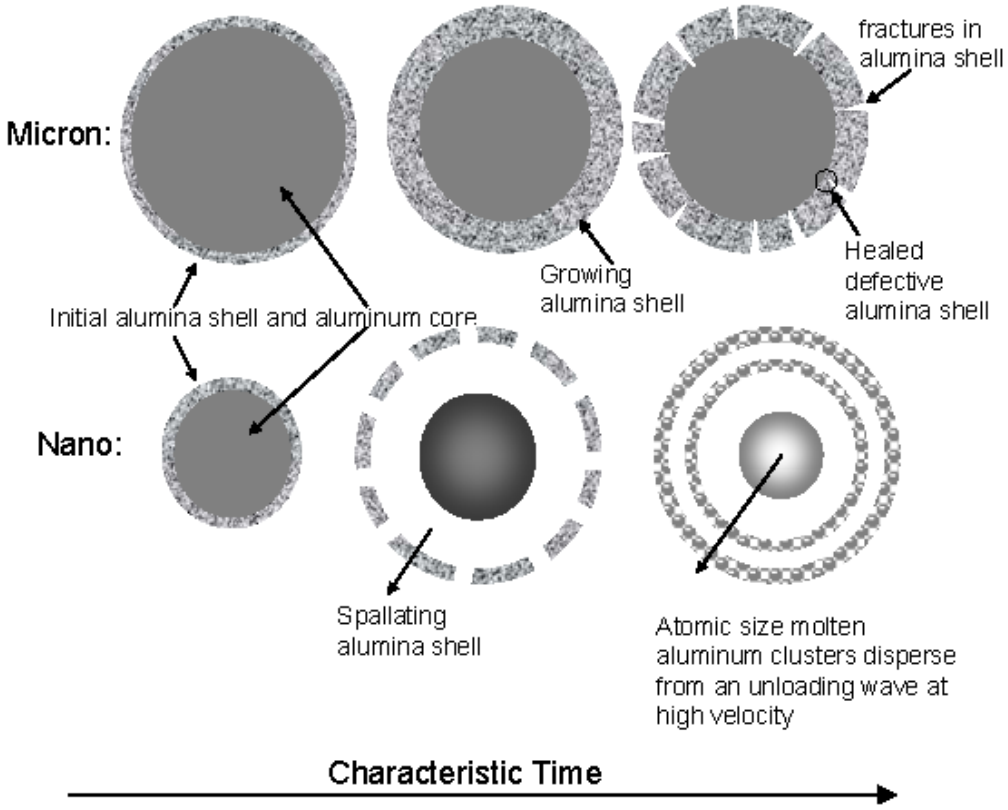

Figure 4. Micron particles react by diffusion of atoms through an oxide shell, which fractures before Al melting and then heals. Nanoparticles react by a melt-dispersion-mechanism where melting of Al creates huge pressure, the oxide shell spallates exposing the molten core and creates an unloading tensile pressure wave which disperses atomic size Al clusters. Reaction of these clusters is not limited by diffusion. This mechanism explains numerous puzzles in nano Al combustion (adopted from [32]).

Sublimation via virtual melting. In the field of tensile stresses and hot spots within a solid (e.g., in a tensile wave [32] or in laser ablation), solid is unstable with respect to gas; however, an activation barrier caused by high solid-gas surface energy suppresses sublimation. Solid-liquid interface energy is usually an order of magnitude smaller than solid-gas energy, and activation energy is proportional to the cube of surface energy. That is why it is quite probable that the *V M* will occur in a small volume as a first kinetically favorable step. Then, either melt vaporizes or decohesion along the solid-melt interface occurs. After decohesion, a void appears due to plastic deformation, and melt evaporates into free space, producing thermodynamically stable gas. We are not aware, however, of any publications that have pursued this idea.

4. Concluding remarks

The developed theory and revealed phenomena in high pressure mechanochemistry can find applications in interpretation of geophysical experiments, friction and wear, mechanical alloying and strain-induced material synthesis. The above examples demonstrate that there are data indicating that the *V M* may be a general phenomenon for various SCs in wide class of solids. Recently, we developed one more example of the hidden mechanochemistry, namely a reaction mechanism of *Al* nanoparticles based on the dispersion of liquid metal [32].

Acknowledgements

Support from the NSF (CMS-02011108 and CMS-0555909), LANL (8060,52844,13720, and 31553), ONR (N000140710318) and TTU is acknowledged. Contributions of all my co-authors are gratefully appreciated.

References

1. Levitas V I 2004 Continuum Mechanical Fundamentals of Mechanochemistry *High Pressure Surface Science and Engineering* eds Y Gogotsi and V Domnich (Institute of Physics, Bristol) Section 3 159-292.
2. Levitas V I 2004 *Phys. Rev. B* **70** 184118.
3. Blank V D, Boguslavski Yu Ya, Eremetz M I et al. 1984 *JEPT* **87** 922.
4. Blank V D, Popov M, Buga S G, Davydov V et al. 1994 *Physics Letters* **A 188** 281.
5. Zharov A A 1994 *High Pressure Chemistry and Physics of Polymers*, ed A L Kovarskii, Ch. (Florida: CRC Press, Boca Raton) p 267-301.
6. Levitas V I 1998 *Int. J. Solids and Structures* **35** 889.
7. Levitas V I 2000 *Int. J. Plasticity* **16** 805 and 851.
8. Levitas V I and Zarechnyy O M 2006 *J. Physical Chemistry* B **110** 16035.
9. Levitas V I and Zarechnyy O M 2007 *Appl Phys. Lett.* **91** 141919.
10. Novikov N V et al. 1999 *Diamond and Related Materials* **8** 361.
11. Levitas V I and Shvedov L K 2002 *Phys. Rev. B* **65** 104109.
12. Levitas V I, Ma Y and Hashemi J 2005 *Appl. Phys. Letters* **86** 071912.
13. Levitas V I, Ma Y, Hashemi J, Holtz M, and Guven N 2006 *J. Chem. Phys.* **25** 044507.
14. Ma Y, Selvi E, Levitas V I and Hashemi J 2006 *J Phys: Cond Matt* **18** 1075.
15. Levitas V I, Henson B F, Smilowitz L B and Asay B W 2004 *Phys. Rev. Lett.* **92** 235702.
16. Levitas V I 2005 **Phys. Rev. Lett. 95** 075701.
17. Levitas V I, Henson B, Smilowitz L and Asay B 2006 *J. Phys. Chem. B* **110** 10105.

18. Levitas V I, Smilowitz L, Henson B and Asay B W 2006 *Appl. Phys. Lett.* **86** 231930.
19. Henson B F, Smilowitz L B, Asay B W and Dickson P M 2002 *J. Chem. Phys.* **117** 3780
20. Smilowitz L, Henson B F, Asay B W and Dickson P M 2002 *J. Chem. Phys.* **117** 3789.
21. Mishima O 1996 *Nature* **384** 546.
22. Brazhkin V V, Lyapin A G et al. 1995 *Phys. Rev. B* **51** 7549.
23. Levitas V I and Ravelo R 2008 *Proc. Plasticity'08, Hawaii* ed A Khan.
24. Jaramillo E, Sewell T D and Strachan A 2007 *Phys. Rev. B* **76** 064112.
25. Hammerberg J E, Ravelo R, Germann T C et al. 2003 *Shock Compression of Condenced Matter: AIP Conf. Proc.* 706 ed M D Furnish et al. 565.
26. Ikeda H, Qi Y et al. 1999 *Phys. Rev. Lett.* **82** 2900.
27. Okamoto P R et al. 1998 *Appl Phys Lett* **73** 473.
28. Lynden-Bell R M 1995 *J. Phys.: Condens. Matter* **7** 4605.
29. Mott N F 1948 *Proceedings of the Physical Society* **60** 391.
30. Schonfelder B et al. 1997 *Interface Science* **5** 245
31. Wolf D 2001 *Current Opinion Solid State and Mat. Sci.* **5** 435.
32. Levitas V I, Asay B W, Son S F and Pantoya M 2007 *J. Appl. Phys.* **101** 083524.